Geophysical Research Letters

RESEARCH LETTER
10.1029/2019GL083574

Climate Sensitivity on Geological Timescales Controlled by Nonlinear Feedbacks and Ocean Circulation

A. Farnsworth[1], D. J. Lunt[1], C. L. O'Brien[2], G. L. Foster[3], G. N. Inglis[4], P. Markwick[5], R. D. Pancost[4], and S. A. Robinson[6]

[1]School of Geographical Sciences and Cabot Institute, University of Bristol, Bristol, UK, [2]Department of Geology and Geophysics, Yale University, New Haven, CT, USA, [3]Ocean and Earth Science, University of Southampton, Southampton, UK, [4]School of Earth Sciences, School of Chemistry, and Cabot Institute, University of Bristol, Bristol, UK, [5]Knowing Earth Ltd, UK, [6]Department of Earth Sciences, University of Oxford, Oxford, UK

Key Points:
- Climate sensitivity on geological timescales depends on continental configuration
- Ocean area and ocean circulation nonlinearly determine climate and climate sensitivity
- Past climate sensitivity is not necessarily a good analogue for future climate sensitivity

Supporting Information:
- Supporting Information S1

Correspondence to:
D. J. Lunt,
d.j.lunt@bristol.ac.uk

Citation:
Farnsworth, A., Lunt, D. J., O'Brien, C. L., Foster, G. L., Inglis, G. N., Markwick, P., et al. (2019). Climate sensitivity on geological timescales controlled by nonlinear feedbacks and ocean circulation. *Geophysical Research Letters*, *46*, 9880–9889. https://doi.org/10.1029/2019GL083574

Received 19 OCT 2018
Accepted 9 JUL 2019
Accepted article online 29 JUL 2019
Published online 20 AUG 2019

Abstract Climate sensitivity is a key metric used to assess the magnitude of global warming given increased CO_2 concentrations. The geological past can provide insights into climate sensitivity; however, on timescales of millions of years, factors other than CO_2 can drive climate, including paleogeographic forcing and solar luminosity. Here, through an ensemble of climate model simulations covering the period 150–35 million years ago, we show that climate sensitivity to CO_2 doubling varies between ~3.5 and 5.5 °C through this time. These variations can be explained as a nonlinear response to solar luminosity, evolving surface albedo due to changes in ocean area, and changes in ocean circulation. The work shows that the modern climate sensitivity is relatively low in the context of the geological record, as a result of relatively weak feedbacks due to a relatively low CO_2 baseline, and the presence of ice and relatively small ocean area in the modern continental configuration.

1. Introduction

Climate sensitivity, in its very broadest terms, is a measure of the response of the climate system to an external forcing. More specifically, it is defined as the global annual mean near-surface air temperature equilibrium response to a defined forcing, usually either 1 W/m^2 (e.g., PALAEOSENS Project Members, 2012) or a doubling of CO_2 (~3.7 W/m^2, e.g., Charney et al., 1979). Despite (or perhaps due to) its simplicity, it is a widely used metric and is a key variable in many impact (e.g., Donner et al., 2005), policy (e.g., Rogelj et al., 2014), and economic (e.g., Hope, 2006) assessments. The Intergovernmental Panel on Climate Change (2013) assesses that climate sensitivity (defined in terms of a doubling of CO_2) is likely to be in the range 1.5 to 4.5 °C, very unlikely to be more than 6 °C, and extremely unlikely to be less than 1 °C.

Given the societal importance of climate sensitivity, it is unsurprising that many studies have turned to observations of past climates in an attempt to further refine, and test, estimates of this key parameter (e.g., see reviews by Rohling et al., 2018; Schmidt et al., 2014). Any such paleofocused attempt to characterize climate sensitivity requires knowledge of (a) the magnitude of the climatic response to a particular forcing and (b) the magnitude of the forcing itself. As such, many attempts to characterize climate sensitivity from the geological record have focused on the relatively recent past, such as the Last Glacial Maximum (e.g., Crucifix, 2006; Hansen et al., 2008; Hargreaves et al., 2012), or the Pleistocene (e.g., Friedrich et al., 2016; Kohler et al., 2018) where data sets for temperature change have relatively good spatial coverage, and the forcings are well understood and quantifiable. However, such studies still have relatively large uncertainties due to difficulties associated with the interpretation of paleoproxy records and/or have often conflated feedbacks and forcings and so have either underestimated or overestimated sensitivity (PALAEOSENS Project Members, 2012). Furthermore, the forcing during the Last Glacial Maximum and much of the Pleistocene was negative relative to modern, and so the relevance for future climate change, where forcing is positive, may be limited. Other studies have focused on warm periods within the last 5 million years, such as the Pliocene (e.g., Hargreaves & Annan, 2016; Haywood et al., 2013; Lunt et al., 2010; Martínez-Botí et al., 2015), when CO_2 concentrations were similar to that of today; however, even these studies do not explore CO_2 concentrations of ~560 ppmv and above, that are more relevant to climate sensitivity and typical end-of-century scenarios (Moss et al., 2010).

More recently, the community has started to move to "deep-time" (here defined as time periods older than ~5 million years ago) warm climates, during which CO_2 concentrations were very high (~1,000 ppmv or more), in an attempt to find time periods where the climate signal and forcings were largest, with the expectation that signal-to-noise ratio will be reduced and climate sensitivity estimates will be more robust (e.g., Anagnostou et al., 2016; Cramwinckel et al., 2018; Shaffer et al., 2016; Zeebe et al., 2009). However, many such time periods were essentially free from continental ice sheets, and tectonic changes over millions of years mean that continental positions, mountain ranges, and ocean bathymetry were all very different compared to modern (e.g., Markwick, 2007). As such, it is possible that estimates of paleo climate sensitivity from these time periods may have limited relevance for assessing modern climate sensitivity, if climate sensitivity is paleogeography dependent. Furthermore, the upper end of CO_2 concentrations during many of these time periods are so high that nonlinearities in forcings and feedbacks (Bloch-Johnson et al., 2015; Caballero & Huber, 2013) may further complicate their relationship to the short-term future.

2. Methods

In order to explore the evolution of climate and climate sensitivity over geological timescales, we carry out an ensemble of 19 pairs of fully coupled atmosphere-ocean-vegetation climate model simulations with varying paleogeography and solar luminosity appropriate for each geological stage from the earliest Cretaceous (Berriasian stage, ~143 Ma) to the latest Eocene (Priabonian stage, ~36 Ma), at ×2 and ×4 preindustrial atmospheric CO_2 concentrations (i.e., 560 and 1,120 ppmv).

The climate model and the ×4 simulations are identical to those described in detail in Lunt et al. (2016), except that here they have been run for longer (10,422 years here compared with 1,422 years), in order to approach more closely to equilibrium, and they use the fully dynamic mode (as opposed to equilibrium mode) of vegetation model.. The ×2 simulations are branched off from the ×4 simulations after 422 years and run for 10,000 years. The only difference between the simulation of each stage relative to another stage is the prescribed paleogeography (see Figure S1 in the supplement of Lunt et al., 2016) and the solar constant (see Figure 2 of Lunt et al., 2016). All simulations have a modern astronomical configuration and are initialized from a homogeneous global ocean salinity and an idealized zonal mean ocean temperature structure, which is a cosine function of latitude (see section 2.5 of Lunt et al., 2016).

The climate model used for the simulations is very similar to the HadCM3BL-M2.1aD model described and evaluated in Valdes et al. (2017), except that we include a modification to the ozone profile to ensure that the model does not develop a runaway warming at ×4 CO_2, as discussed in Lunt et al. (2016). The model includes representations of "Charney" feedbacks associated with changes in clouds, snow/seaice, lapse rate and water vapor, and the "Earth system" feedback associated with changes in vegetation (Lunt et al., 2010), but does not include many other Earth system feedbacks associated with changes to, for example, dust, methane, nitrogen dioxide, or ozone. The sign of many of these missing feedbacks is uncertain (Intergovernmental Panel on Climate Change, 2013), so it is not clear if our simulations will over or underestimate "true" long-term Earth system sensitivity.

At the end of the model integration, all the simulations are very well spun up, with only small residual trends in ocean temperature, even in the deep ocean (the mean absolute global mean temperature trend at 2,700-m depth of all simulations in the last 1,000 years of simulation is 0.06 °C per millennium; see supporting information Figure S1). In addition, Gregory plots (Gregory et al., 2004) of the energy balance at the top of the atmosphere (TOA) against global mean surface temperature (supporting information Figure S2) show that the energy balance is very close to zero for all simulations and that any residual energy balance is decreasing over time (the mean absolute TOA inbalance across all simulations is 0.036 W/m^2, and the maximum TOA inbalance is +0.09 W/m^2 in the Cenomanian at ×4). However, there is a drift in the global mean salinity due primarily to the rigid-lid approximation in the ocean model, which includes minimum and maximum salinity thresholds (0 and 45 psu, respectively). This, coupled with the presence of enclosed or restricted basins (such as the Arctic Ocean) with a net input of freshwater from the surrounding river catchments, means that the restricted basins become very fresh and reach the minimum salinity threshold at the surface while the rest of the ocean tends to increase in salinity. We do not expect this drift to affect our results because (i) the absolute salinity does not have a strong effect on the density gradients due to the linearity of the equation of state (Bryan & Cox, 1972) in the regime of the majority of the global ocean, (ii) the enclosed basins that reach the minimum salinity threshold have a relatively small area and do not affect the global

ocean circulation, and (iii) the maximum salinity threshold is only reached in a few isolated grid cells in the tropics in the later Eocene simulations (supporting information Figure S3). Indeed, the mixed layer depths in our simulations (supporting information Figure S6) are very similar to those presented in Lunt et al. (2016, their supplement Figure S10), indicating that the ocean circulation is relatively unchanged after 9,000 years, despite the gradual drift in salinity and gradually equilibrating temperatures.

3. Results

3.1. Climate and Climate Sensitivity

Figure 1a shows the global annual mean near-surface air temperature for the high (×4) and low (×2) CO_2 simulations (and see Table S1 in the supporting information). Both sets of simulations show a similar trend (the r correlation coefficient between the two time series is 0.86; supporting information Figure S4). In particular, there is a cooling in the very earliest Cretaceous between the Berriasian and Valanginian at 140 Ma, a warming from ~130 to 90 Ma peaking at the Turonian, and a cooling from 90 to 80 Ma to a minimum in the Campanian. In the Paleocene and Eocene the trends are less consistent across the two sets of simulations, but include a maximum in the Ypresian.

The global mean temperature in our ×4 simulations has a greater total range across the geological stages than that in the shorter simulations of Lunt et al. (2016; ~3 °C compared with ~1 °C; compare our Figure 1 with their Figures 5 and 7), and the regional expression of this range also differs, but the main conclusion of Lunt et al. (2016), that changes in paleogeography have a substantial effect on regional climate that must be considered when interpreting long proxy records, is robust.

Figure 1b shows the climate sensitivity of each stage (the difference in global mean temperature between the ×2 and ×4 simulations); regional plots are shown in supporting information Figure S5. The mean climate sensitivity over this period is 4.2 °C, the minimum is 3.7 °C (Berriasian stage, ~145 Ma), and the maximum is 5.3 °C (Maastrichtian stage, ~70 Ma). The change in global climate sensitivity over time includes a gradual increase in sensitivity from the earliest Cretaceous to the latest Cretaceous, a decrease to a minimum in the Paleocene, and then an increase followed by a decrease in the Eocene. Our modeled range of climate sensitivities in the Eocene (3.8 to 4.7 °C) is consistent with estimates of 3.5 to 8.9 °C (Cramwinckel et al., 2018) and 2.9 to 4.0 °C (Anagnostou et al., 2016), inferred from temperature and CO_2 proxies for this time period.

A quantitative analysis of the driving mechanisms is carried out in section 3.2, but in qualitative terms, the global mean temperature in the simulations appears to be driven by a combination of CO_2 (explaining the offset in temperature between ×2 and ×4), increasing solar constant (explaining a general increase in temperature from the earliest Cretaceous to latest Eocene in both ×2 and ×4), plus a more variable signal that must be associated with changing paleogeography. This paleogeographic signal appears to be strongly related to the area of ocean in the prescribed paleogeographies (Figure 1c); the ocean area correlates with both the ×4 (r correlation coefficient = 0.63) and ×2 simulations (r correlation coefficient = 0.42). The mechanism for this paleogeographic forcing is discussed in section 3.2.

However, there are some differences between ×2 and ×4 that do not fit this qualitative relationship and that can be seen in the evolution of climate sensitivity. In particular, there is a large swing in sensitivity around the Cretaceous-Paleocene boundary, with relatively high sensitivity at the Maastrichtian and low sensitivity in the Selandian, due to a relatively warm Maastrichtian at ×4 and a relatively warm Selandian at ×2 (Figures 1a and 1b). These anomalies are associated with changes in ocean circulation that take place as a function of CO_2 at these two stages (supporting information Figure S6). The ocean circulation around this time has two possible states: (i) a relatively warm global state characterized by deep water formation in the south Pacific Ocean (Maastrichtian at ×4 and Selandian at ×2; supporting information Figures S6b and S6g) and (ii) a relatively cold global state characterized by deep water formation in the South Atlantic and Indian Oceans (Maastrichtian at ×2 and Selandian at ×4; supporting information Figures S6c and S6f). Although changes in ocean circulation may not be expected to affect the global mean temperature to a great extent, in this case increased poleward heat transport in the Pacific basin results in a greater increase in global mean temperature than that caused by increased poleward heat transport in the Atlantic/Indian basins. This enhanced Pacific poleward heat transport may be related to the greater areal extent of the Pacific basin and is enhanced by sea ice albedo feedbacks around Antarctica. As such, the Cretaceous-Paleocene boundary is a particularly sensitive time period to relatively small changes in paleogeography and/or CO_2, resulting in

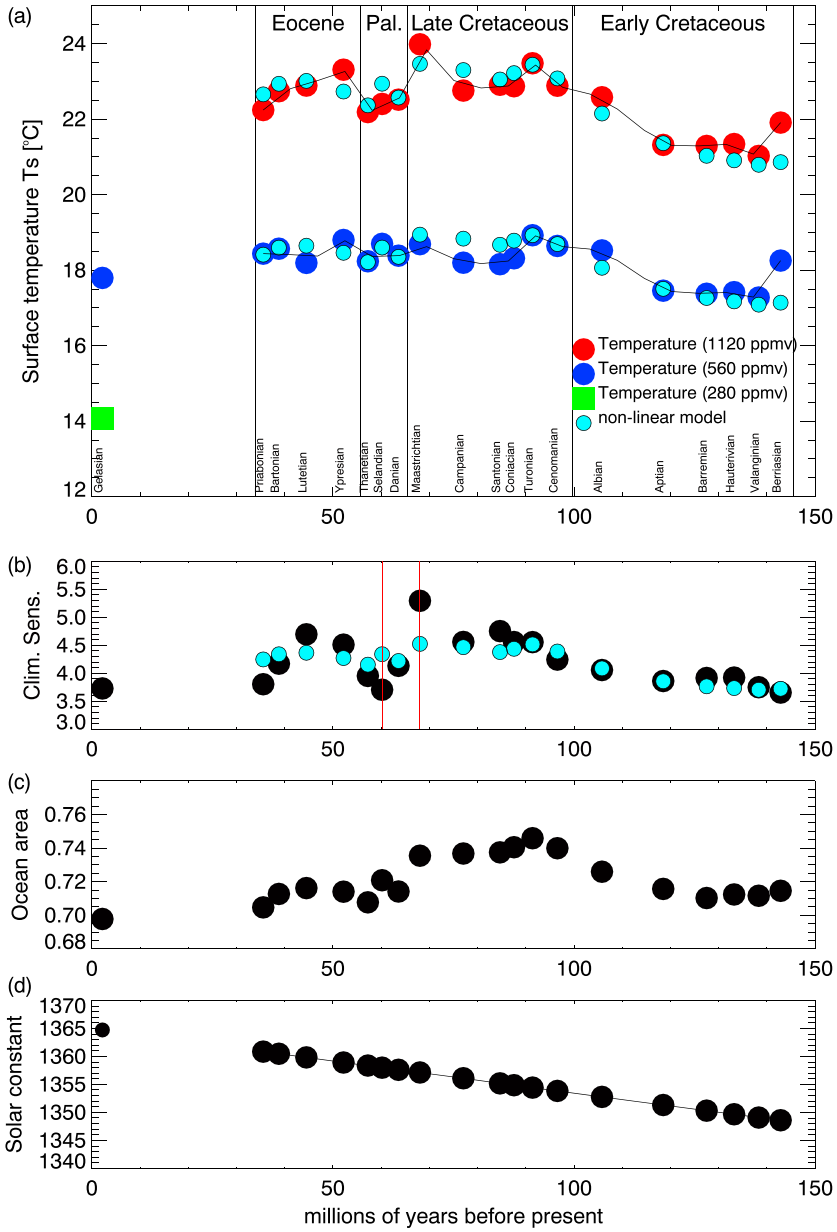

Figure 1. (a) Global annual mean near-surface air temperature in the ×2 (dark blue circles) and ×4 (red circles) CO_2 simulations, and the Gelasian ×1 simulation (green square). For each set of simulations the curved black line is a spline fit to the data, of resolution about 5 million years. The nonlinear model fit to the ×2, ×4 simulations is shown with light blue circles. (b) Global mean climate sensitivity (i.e., ×4 minus ×2) over time (black circles). Nonlinear model sensitivity is shown with light blue circles. Red vertical lines show those time periods that have a switch in ocean circulation between the ×2 and ×4 simulations. (c) Ocean area over time (as a fraction of the global surface area, calculated from the paleogeographies at the model resolution). (d) Solar constant over time (W/m^2).

anomalously large or small climate sensitivities. For all other time periods, the deep water formation occurs in the same regions at ×4 as at ×2, although the region varies as a function of paleogeography (e.g., in the South Atlantic in the Priabonian, supporting information Figures S6a and S6e; in the North Pacific in the Berriasian, supporting information Figures S6d and S6h).

3.2. Quantitative Role of Nonlinear Feedbacks in Determining Climate Sensitivity

As well as the qualitative considerations above, a quantitative analysis of the simulations is also possible. Here, we focus on the global mean response through application of a radiative forcing and feedback framework. Traditional linear radiative forcing theory (Hansen et al., 1984) states that if we choose one simulation

as a reference state, all other simulations can be considered as a perturbation to this reference state, caused by a forcing F_{all} (W/m^2), where F_{all} is the sum of three separate forcings: F_{co2} due to a change in CO_2, F_{solar} due to a change in solar constant, and F_{geog} due to a change in paleogeography. Furthermore, the temperature difference relative to the reference state, ΔT, is given by

$$\Delta T = -\frac{F_{all}}{\lambda} = -\frac{F_{co2} + F_{solar} + F_{geog}}{\lambda}, \quad (1)$$

where λ, the feedback parameter (W $\cdot$ m$^{-2}\cdot$K^{-1}), is negative. If we choose the Turonian at ×2 as our reference simulation, then F_{co2} is 0 for all the ×2 simulations and equal to ΔR for all the ×4 simulations, where ΔR is the radiative forcing for a doubling of CO_2. F_{solar} can be approximated by $(1 - \alpha_p)\Delta S_0/4$, where ΔS_0 is the change in solar constant relative to the Turonian and α_p is the planetary albedo. For the paleogeographic forcing, F_{geog}, the apparent importance of ocean area discussed in section 3.1 suggests a role for surface albedo radiative forcing. Using a simple energy balance model, Barron et al. (1980) showed that the albedo forcing, due to changes in continental versus ocean area caused by changes in sea level, had a substantial effect on global mean temperature on geological timescales. The importance of ocean area through surface albedo forcing is also supported by more recent work (Pohl et al., 2019). However, others have suggested that the primary role of paleogeography on global mean temperature is through seasonality effects associated with the degree of fragmentation of continents (Donnadieu et al., 2006; Ladant & Donnadieu, 2016). Nonetheless, assuming changes in surface albedo to be the primary forcing due to paleogeography, F_{geog}, can be approximated by $\Delta\alpha_s S_0/4$, where $\Delta\alpha_s$ is the change in surface albedo relative to the Turonian.

However, this linear framework predicts climate sensitivity to be constant over geological time, because for each pair of ×2, ×4 simulations, the only difference in forcing is equal to ΔR, which is constant, giving a constant climate sensitivity of $-\Delta R/\lambda$. This is clearly at odds with the variable climate sensitivity in the full climate model (Figure 1c), as also highlighted by the non-unity slope of the best fit line between the ×2 and ×4 simulations (supporting information Figure S4). As such, we introduce a nonlinear parameter, a (W$\cdot$m$^{-2}\cdot$K^{-2}), into equation (1), following Bloch-Johnson et al. (2015), such that

$$-F_{all} = \lambda\Delta T + a\Delta T^2. \quad (2)$$

The parameter a represents a temperature dependence (i.e., a nonlinearity) of the strength of the feedbacks. Solving the resulting quadratic equation, and taking the physically realistic negative root, gives

$$\Delta T = \frac{-\lambda - \sqrt{\lambda^2 - 4a(F_{co2} + e_{solar}F_{solar} + e_{geog}F_{geog})}}{2a}, \quad (3)$$

where we have included factors e_{solar} and e_{geog}, which allow the efficacy (i.e., the temperature response due to a unit forcing, Hansen et al., 2005) of the solar and paleogeography terms to differ from that of CO_2 (for which the efficacy is equal to 1). In order to calculate the CO_2 forcing (F_{CO2}) and the solar forcing (F_{solar}) we take $\Delta R = 3.7$ W/m^2 (Houghton et al., 2001) and ΔS_0 from the solar constants prescribed in each simulation (Figure 1d). For the paleogeographic forcing (F_{geog}), we simply assume that the surface albedo change, $\Delta\alpha_s = (\alpha_l - \alpha_o)\Delta A_o$ where $\alpha_l = 0.14$ and $\alpha_l = 0.06$ are typical global mean albedos of land and ocean, respectively, in the simulations, and ΔA_o is the relative change in area of ocean given in Figure 1c. In order to account for the greater impact on radiative forcing of albedo changes in the tropics, we calculate the paleogeographic forcing as a function of latitude, accounting for varying incoming solar radiation, and weighting by area. This leaves equation (3) with four unknowns; λ, a, e_{solar}, and e_{geog}. A minimal subjective tuning shows that $\lambda = -1$ W$\cdot$m$^{-2}\cdot$K^{-1}, $a = 0.04$ W$\cdot$m$^{-2}\cdot$K^{-2}, $e_{solar} = 0.7$, and $e_{geog} = 1.25$ gives a good qualitative match to our results for absolute temperature at ×2 and ×4, and climate sensitivity (Figures 1a and 1b, light blue circles). Two exceptions are the Maastrichtian and Selandian stages, which we have already shown are associated with changes in the mode of ocean circulation, which are not captured in this simple forcings/feedbacks framework. We note that $\lambda = -1$ W$\cdot$m$^{-2}\cdot$K^{-1} corresponds to a linear climate sensitivity of 3.7 °C per CO_2 doubling, which is within the range estimated by the IPCC. We also note that $a = 0.04$ W$\cdot$m$^{-2}\cdot$K^{-2} is within the range estimated by Bloch-Johnson et al. (2015) of $-0.04 \leq a \leq 0.06$ W$\cdot$m$^{-2}\cdot$K^{-2} from various climate model simulations carried out at multiple CO_2 concentrations. Finally, we note that a value of e_{geog} close to unity also supports the assumption that surface albedo forcing associated with ocean area is a mechanism for variations in F_{geog} that is consistent with simple radiative forcing considerations. In principle, these four unknowns (λ, a, e_{solar}, and e_{geog}) could be objectively tuned to give a best fit to the data in Figure 1; however,

here we are most interested in the general principle, which is that the evolution in climate sensitivity can be explained by nonlinear feedbacks in the framework of Bloch-Johnson et al. (2015). It is worth noting that, as discussed by Bloch-Johnson et al. (2015), a negative term inside the square root in equation (3) can be interpreted as the system developing a runaway greenhouse. For our values of λ and a, this occurs at a total forcing of +6.25 W/m^2 relative to the Turonian at ×2, or about 1,800 ppmv of CO_2.

In order to explore the origin of these nonlinear feedbacks on a global scale, we carry out a zonal mean energy balance analysis of the simulations, following Heinemann et al. (2009). This shows that both albedo changes and emissivity changes contribute to the nonlinearity in response to the solar and paleogeographic forcing. Given the relative warmth of the deep-time model simulations, it is likely that the nonlinearity in albedo response is driven by nonlinearities in short wave cloud feedbacks, rather than snow and sea ice feedbacks. Indeed, regionally it is the tropics that dominate the nonlinearity in climate sensitivity (supporting information Figures S7a–S7c).

The changes in ocean area are dominated by changes in the Northern Hemisphere midlatitudes; the maximum in ocean area is during the Turonian (mid-Cretaceous) when the Western Interior Seaway in North America is extensive (see Figure S1 in the supplement of Lunt et al., 2016). The ocean area in the paleogeographies is consistent with sea level reconstructions of the Phanerozoic, such as Müller et al. (2008), derived primarily from the age-area and depth-area distribution of the modern-day ocean floor. These reconstructions also show a maximum in the mid-Cretaceous; this agreement is unsurprising given that sea level reconstructions inform the production of the paleogeographies. However, the details of the coastlines in the paleogeographies are uncertain, in particular for greenhouse climates (Sømme et al., 2009).

Furthermore, the nonlinearity found in our simulations supports previous studies that found that past climate sensitivity was a function of baseline CO_2 (e.g., Pohl et al., 2014, for the Ordovician) and suggests that further nonlinear behavior would occur if we carried out simulations at ×1 or ×8 CO_2.

3.3. Implications for Assessment of Future Climate Sensitivity

It has been proposed that observational evidence of the climate sensitivity of the past may be useful for constraining future climate sensitivity. To test this hypothesis, we explore the relationship between modern and past climate sensitivity. To this end, in addition to the Cretaceous, Paleocene, and Eocene simulations discussed above, we also carry out a pair of Gelasian (early Pleistocene, ~2 Ma) simulations, spun up in an identical manner to the other simulations, but at CO_2 concentrations of ×1 and ×2 (Figure 1a). The Gelasian is the closest available paleogeography to modern that has been produced using the same procedures as the deep-time paleogeographies. In addition to the solar constant, paleogeography and CO_2, this pair differs from the others in that it has extensive Antarctic and Greenland ice sheets. The Gelasian climate sensitivity (3.7 °C) is at the lower end of the ensemble. Given the dependence of climate sensitivity on temperature (i.e., the nonlinearity of climate sensitivity) in the model simulations, this implies that for the modern, the relatively small ocean area (Figure 1c) combined with the presence of the Antarctic and Greenland ice sheets, more than offsets the relatively high solar constant (Figure 1d), resulting in a relatively low climate sensitivity (and relatively cold ×2 simulation in the context of the increasing trend through the Cretaceous-Paleocene-Eocene). The fact that CO_2 increases from ×1 to ×2 rather than ×2 to ×4 likely plays an additional role in the low modern sensitivity, through nonlinearities in both feedbacks and CO_2 forcing (Caballero & Huber, 2013). The regional expression of climate sensitivity in the Gelasian includes an area of cooling in the North Pacific (supporting information Figure S5a), but this does not appear to be associated with changes in deep water formation. Cooling in this region is not seen in CO_2-doubling model simulations associated with CMIP5 (Intergovernmental Panel on Climate Change, 2013). This could either be because the Gelasian has some paleogeographic differences to modern (notably, land in the region of what is today the Barents Sea, absence of a Hudson Bay, and a slightly open Panama Seaway), or because these simulations are run much longer than CMIP5 simulations. If we take the Gelasian results as representative of the modern climate sensitivity, then the implication is that the use of observational geological data from the Cretaceous, Paleocene, or Eocene (e.g., Anagnostou et al., 2016; Cramwinckel et al., 2018) to constrain future climate sensitivity should be carried out with care and could in general lead to higher estimates than are appropriate for modern. Indeed, the dependence of feedbacks on baseline temperature highlighted in this work provide a plausible explanation for why Anagnostou et al. (2016) found a higher climate sensitivity (~4 °C per CO_2 doubling) in the relatively warm early Eocene climatic optimum than in the relatively cool late Eocene (~3 °C per CO_2 doubling). Our findings are also consistent with Cramwinckel et al. (2018, their

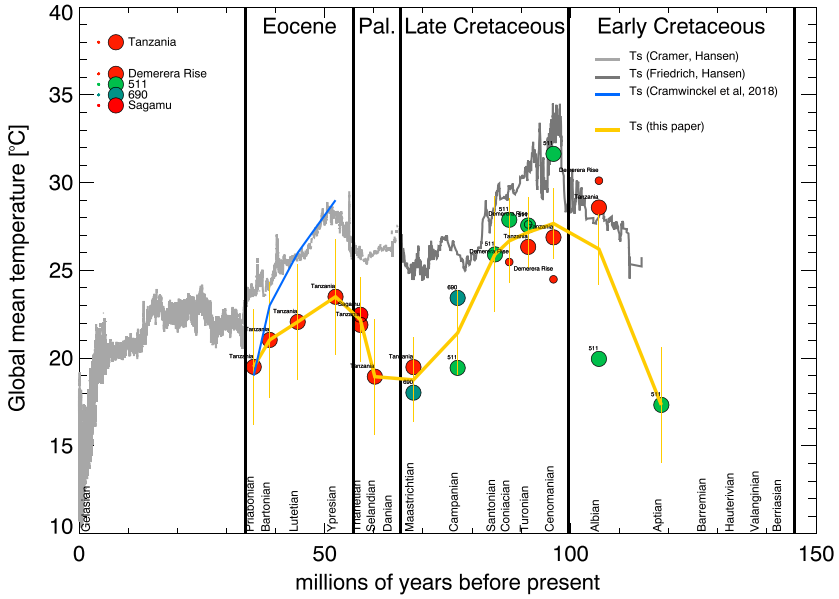

Figure 2. Filled circles show the global mean temperature inferred from the model simulations and planktic δ^{18}O sea surface temperature estimates from the sites in the supporting information Figure S8 (using equation (4), as illustrated in Figure S9). The color corresponds to the modern latitude of each site, with warm colors for low latitudes and cold colors for high latitudes. Smaller circles are those sites where the paleorotations are approximate. The orange curve shows the mean inferred temperature for each geological stage, with uncertainty bars according to the number of sites (see supporting information Figure S10). The gray lines are global mean temperatures estimated from the Cramer et al. (2011; light gray) and Friedrich et al. (2012; dark gray) benthic δ^{18}O data sets, using the method of Hansen et al. (2013). The blue line shows global mean temperatures in the Eocene from Cramwinckel et al. (2018).

Extended Data Figure 9), who, relative to the late Eocene, find a higher sensitivity for the warm EECO than for the cooler middle Eocene.

3.4. Model Evaluation: Inference of Global Mean Temperature From Single-Site Proxy SST Data and Comparison With Benthic Records

The simulations cannot be directly evaluated with paleoclimate temperature data, because CO_2 records of this time period are relatively uncertain (Foster et al., 2017). However, in combination with proxy sea surface temperature (SST) records derived from planktic δ^{18}O from individual sites, the simulations can be used to infer a global mean temperature, which can itself be compared with global mean temperature derived from independent benthic δ^{18}O records (Figure 2), providing an evaluation of the regional signals in the model simulations.

We assume that the global mean temperature and local SST scale linearly with each other, with a scaling factor derived from our model simulations at the two CO_2 concentrations. As such, if the modeled temperature at the location of the proxy temperature (taking into account appropriate paleorotations due to plate movements), at the two different CO_2 concentrations, is T^{2x} and T^{4x}, and the modeled global mean temperature at these CO_2 concentrations is $< T^{2x} >$ and $< T^{4x} >$, then the inferred global mean temperature, $< T >^{\text{inferred}}$, can be derived from the proxy temperature estimate T_{proxy}, as

$$< T >^{\text{inferred}} = < T^{2x} > + (T^{\text{proxy}} - T^{2x}) \frac{< T^{4x} > - < T^{2x} >}{T^{4x} - T^{2x}}. \quad (4)$$

Note that if the proxy temperature is greater than T^{4x}, or cooler than T^{2x}, then the inferred global mean is found by extrapolation rather than by interpolation and is therefore more uncertain (see supporting information Figure S9). This is typically for inferred temperatures above about 23 °C. The process is illustrated in Figure S9 in the supporting information for three sites.

We take T_{proxy} from planktic δ^{18}O estimates of Cretaceous, Paleocene, and Eocene SST compiled in O'Brien et al. (2017; their Figure 9b) and Cramwinckel et al. (2018; supporting information Figure S8a; the modern site locations and their paleorotations are shown in Figure S8b). Prior to calculating $< T^{\text{inferred}} >$, we remove

planktic δ^{18}O records from one location (Blake Nose, sites 1050 and 1052) that appear exceptionally cold biased, which we suggest potentially results from diagenesis. The $< T >^{\text{inferred}}$ for each site is shown in Figure 2 as filled circles for each site (for some sites, the paleorotations do not extend back as far as the SST data; for these sites, shown as smaller circles, the last existing location is used), and the mean for each stage as an orange curve (including uncertainty estimates, see Figure S10 in the supporting information). The inferred global means from each site are less scattered than the SSTs from each site (supporting information Figure S8a), implying that our inference process has some skill in reconciling individual SST records.

The inferred global mean temperature is for comparison with global mean temperature derived from the benthic δ^{18}O data of Cramer et al. (2011) and Friedrich et al. (2012), using the method of Hansen et al. (2013) in which benthic δ^{18}O is scaled to global mean temperature using a simple function that depends on the ice volume (Figure 2 in the main paper, gray lines). The $< T >^{\text{inferred}}$ curve shows similar trends to the global mean surface temperature derived from benthic δ^{18}O, namely, a maximum in the mid-Cretaceous (Cenomanian, ~95 Ma), a secondary maximum in the early Eocene (Ypresian, ~50 Ma), and a minimum in the latest Cretaceous (Maastrichtian, ~70 Ma). However, $< T >^{\text{inferred}}$ is cooler than the central Friedrich et al. (2012) estimate by about 5 °C. An offset is not surprising given that the Hansen et al. (2013) methodology makes the simple assumption that changes in global mean surface temperature are identical to changes in benthic ocean temperature prior to the Pliocene. In addition, the Friedrich et al. (2012) benthic δ^{18}O data prior to the Paleocene could be regarded as representing an upper bound on temperature, because much of the warmest underlying data comes from Demerara Rise, which is bathed by a warm, saline water mass forming on the South American shelf (Friedrich et al., 2008; MacLeod et al., 2008). The cooling trend through the Eocene in our $< T >^{\text{inferred}}$ is also seen in the recent estimates of global mean temperature from Cramwinckel et al. (2018; blue line in Figure 2). However, our trend is less pronounced, being cooler in the early Eocene (Ypresian) by about 6 °C.

We also carry out the same process using a combined δ^{18}O and TEX_{86} data set (supporting information Figure S11), using TEX_{86} estimates compiled in O'Brien et al. (2017; their Figure 9b), Inglis et al. (2015), and Cramwinckel et al. (2018), using a linear calibration (supporting information Figures S11a–S11c) and an exponential calibration (supporting information Figures S11c and S11d). This results in inferred temperatures with more variation across different sites than those from solely δ^{18}O, and in particular several sites give very warm inferred temperatures during the Eocene, especially those from the southwest Pacific sector of the Southern Ocean (e.g., ODP Site 1172, Hampden Beach, IODP Site 1356). This may result from a cold model bias in the high latitudes, which has been noted in simulations of the early Eocene with this model (Lunt et al., 2012), or a cold model bias in this particular region (Douglas et al., 2014). However, it may also be in part due to possible seasonal biases in the TEX_{86} data (Sluijs et al., 2006). This possibility is supported by the reversed meridional temperature gradient implied in some sites in the raw TEX_{86} temperatures (e.g., site FL533 in the Campanian, or Mid Waipara in the Ypresian, supporting information Figure S11b). This, combined with recent discussions regarding the interpretation of the TEX_{86} proxy (Ho & Laepple, 2016; Tierney et al., 2017), and the variety of published calibrations (see overview in Inglis et al., 2015), makes interpretation of the resulting apparent inconsistencies challenging. However, it is worth noting that our estimates of inferred global mean temperature from the TEX_{86} proxy at ODP Site 959 in the Eocene are in remarkable agreement with those inferred by Cramwinckel et al. (2018; supporting information Figure S11a).

4. Conclusions

In summary, modeled climate sensitivity varies through the Cretaceous-Paleocene-Eocene from about 3.5 to about 5.5 °C. This variation is explained by a combination of the changing background forcing through this time period due to gradually increasing solar luminosity and varying ocean area and nonlinearities in water vapor and shortwave cloud feedbacks. The maximum in sensitivity in the Maastrichtian can be explained through a combination of its high ocean area and reasonably high solar luminosity, combined with a switch in the mode of ocean circulation. The modern climate sensitivity is relatively low in this context, despite the high solar luminosity, due to its low atmospheric CO_2 baseline, relatively small ocean area, and the presence of ice sheets. The model simulations that underpin these findings cannot be directly evaluated, but the relationship between simulated local and global mean temperatures is consistent with proxy δ^{18}O estimates of SST and deep ocean temperatures. Finally, in the context of future climate sensitivity, this work supports the importance of studies exploring nonlinearities in feedbacks and climate sensitivity in the framework of nonlinMIP (Good et al., 2016).

Acknowledgments
We acknowledge support from the U.K. National Environmental Council Grants NE/K014757/1, NE/I005722/1, NE/I005714/1, NE/K012479/1, NE/I005501/2, and NE/P01903X/1. R. D. P. acknowledges ERC Grant 340923 (TGRES). Figures S1 to S11 are available in the supporting information. The output from the model simulations is available from the https://www.paleo.bristol.ac.uk/ummodel/scripts/papers/Farnsworth_et_al_2019.html website.

References

Anagnostou, E., John, E. H., Edgar, K. M., Foster, G. L., Ridgwell, A., Inglis, G. N., et al. (2016). Changing atmospheric CO_2 concentration was the primary driver of Early Cenozoic climate. *Nature*, *533*, 380–384. https://doi.org/10.1038/nature17423

Barron, E. J., Sloan, J. L. II, & Harrison, C. G. A. (1980). Potential significance of land-sea distribution and surface albedo variations as a climatic forcing factor; 180 m.y. to the present. *Palaeogeography, Palaeoclimatology, Palaeoecology*, *30*, 17–40.

Bloch-Johnson, J., Pierrehumbert, R. T., & Abbot, D. S. (2015). Feedback temperature dependence determines the risk of high warming. *Geophysical Research Letters*, *42*, 4973–4980. Retrieved from https://doi.org/10.1002/2015GL064240

Bryan, K., & Cox, M. D. (1972). An approximate equation of state for numerical models of ocean circulation. *Journal of Physical Oceanography*, *2*, 510–514.

Caballero, R., & Huber, M. (2013). State-dependent climate sensitivity in past warm climates and its implications for future climate projections. *Proc Natl Acad Sci*, *110*, 14,162–14,167.

Charney, J., Arakawa, A., Baker, D. J., Bolin, B., Dickinson, R. D., Goody, R. M., et al. (1979). *Carbon dioxide and climate: A scientific assessment*. Washigton, DC: National Research Council.

Cramer, B. S., Miller, K. G., Barrett, P. J., & Wright, J. D. (2011). Late Cretaceous-Neogene trends in deep ocean temperature and continental ice volume: Reconciling records of benthic foraminiferal geochemistry (δ^{18}o and mg/ca) with sea level history. *Journal of Geophysical Research*, *116*, C12023. https://doi.org/10.1029/2011JC007255

Cramwinckel, M. J., Huber, M., Kocken, I. J., Agnini, C., Bijl, P. K., Bohaty, S. M., et al. (2018). Synchronous tropical and polar temperature evolution in the Eocene. *Nature*, *559*, 382–386.

Crucifix, M. (2006). Does the Last Glacial Maximum constrain climate sensitivity? *Geophysical Research Letters*, *33*, L18701. https://doi.org/10.1029/2006GL027137

Donnadieu, Y., Pierrehumbert, R., Jacob, R., & Fluteau, F. (2006). Modelling the primary control of paleogeography on Cretaceous climate. *Earth and Planetary Science Letters*, *248*, 426–437.

Donner, S. D., Skirving, W. J., Little, C. M., Oppenheimer, M., & Hoegh-Guldberg, O. (2005). Global assessment of coral bleaching and required rates of adaptation under climate change. *Global Change Biology*, *11*, 2251–2265.

Douglas, P. M. J., Affek, H. P., Ivany, L. C., Houben, A. J. P., Sluijs, A., Sijp, W. P., et al. (2014). Pronounced zonal heterogeneity in Eocene southern high-latitude sea surface temperatures. *PNAS*, *111*, 6582–6587.

Foster, G. L., Royer, D. L., & Lunt, D. J. (2017). Future climate forcing potentially without precedent in the last 420 million years. *Nature Communications*, *8*, 14845. https://doi.org/10.1038/ncomms14845

Friedrich, O., Erbacher, J., Moriya, K., Wilson, P., & Kuhnert, H. (2008). Warm saline intermediate waters in the Cretaceous tropical Atlantic Ocean. *Nature Geoscience*, *1*, 453–457.

Friedrich, O., Norris, R. D., & Erbacher, J. (2012). Evolution of middle to late Cretaceous oceans—A 55 m.y. record of Earth's temperature and carbon cycle. *Geology*, *40*, 107–110.

Friedrich, T., Timmermann, A., Tigchelaar, M., Timm, O. E., & Ganopolski, A. (2016). Nonlinear climate sensitivity and its implications for future greenhouse warming. *Science Advances*, *2*, e1501923. https://doi.org/10.1126/sciadv.1501923

Good, P., Andrews, T., Chadwick, R., Dufresne, J.-L., Gregory, J. M., Lowe, J. A., et al. (2016). NonlinMIP contribution to CMIP6: Model intercomparison project for non-linear mechanisms: Physical basis, experimental design and analysis principles (v1.0). *Geoscientific Model Development*, *9*(11), 4019–4028. Retrieved from https://www.geosci-model-dev.net/9/4019/2016/. https://doi.org/10.5194/gmd-9-4019-2016

Gregory, J. M., Ingram, W. J., Palmer, M. A., Jones, G. S., Stott, P. A., Thorpe, R. B., et al. (2004). A new method for diagnosing radiative forcing and climate sensitivity. *Geophysical Research Letters*, *31*, L03205. https://doi.org/10.1029/2003gl018747

Hansen, J., Lacis, A., Rind, D., Russell, G., Stone, P., Fung, I., et al. (1984). Climate sensitivity: Analysis of feedback mechanisms. In J. E. Hansen, & T. Takahashi (Eds.), *Climate processes and climate sensitivity* (pp. 130–163). Washington, DC: American Geophysical Union. ,

Hansen, J., Sato, M., Kharecha, P., Beerling, D., Berner, R., Masson-Delmotte, V., et al. (2008). Target atmospheric CO_2: Where should humanity aim? *The Open Atmospheric Science Journal*, *2*, 217–231.

Hansen, J., Sato, M., Ruedy, R., Nazarenko, L., Lacis, A., Schmidt, G. A., et al. (2005). Efficacy of climate forcings. *Journal of Geophysical Research*, *110*, D18104. https://doi.org/10.1029/2005JD005776

Hansen, J., Sato, M., Russell, G., & Kharecha, P. (2013). Climate sensitivity, sea level and atmospheric carbon dioxide. *Philosophical Transactions of the Royal Society A*, *371*, 20120294.

Hargreaves, J. C., & Annan, J. D. (2016). Could the pliocene constrain the equilibrium climate sensitivity *Climate of the Past*, *12*(8), 1591–1599. https://doi.org/10.5194/cp-12-1591-2016

Hargreaves, J. C., Annan, J. D., Yoshimori, M., & Abe-Ouchi, A. (2012). Can the Last Glacial Maximum constrain climate sensitivity? *Geophysical Research Letters*, *39*, L24702. https://doi.org/10.1029/2012GL053872

Haywood, A. M., Hill, D. J., Dolan, A. M., Otto-Bliesner, B. L., Bragg, F., Chan, W.-L., et al. (2013). Large-scale features of Pliocene climate: Results from the Pliocene model intercomparison project. *Climate of the Past*, *9*(1), 191–209. Retrieved from https://www.clim-past.net/9/191/2013/. https://doi.org/10.5194/cp-9-191-2013

Heinemann, M., Jungclaus, J. H., & Marotzke, J. (2009). Warm Paleocene/Eocene climate as simulated in ECHAM5/MPI-OM. *Climate of the Past*, *5*, 785–802.

Ho, S. L., & Laepple, T. (2016). Flat meridional temperature gradient in the early eocene in the subsurface rather than surface ocean. *Nature Geoscience*, *9*, 606610.

Hope, C. (2006). The marginal impact of CO_2 from PAGE2002: An integrated assessment model incorporating the IPCCs five reasons for concern. *The Integrated Assessment Journal*, *6*, 19–56.

Houghton, J. T., Ding, Y., Griggs, D. J., Noguer, M., van der Linden, P. J., Dai, X., et al. (2001). *Climate change 2001: The scientific basis*. Cambridge, UK: Cambridge University Press.

Intergovernmental Panel on Climate Change (2013). *Climate change 2013: The physical science basis*. Cambridge: Cambridge University Press.

Inglis, G. N., Farnsworth, A., Lunt, D., Foster, G. L., Hollis, C. J., Pagani, M., et al. (2015). Descent towards the icehouse: Eocene sea surface cooling inferred from GDGT distributions. *Paleoceanography and Paleoclimatology*, *30*, 1000–1020. https://doi.org/10.1002/2014PA002723

Kohler, P., Knorr, G., Stap, L. B., Ganopolski, A., de Boer, B., van de Wal, R. S. W., et al. (2018). The effect of obliquity-driven changes on paleoclimate sensitivity during the late pleistocene. *Geophysical Research Letters*, *45*, 6661–6671. https://doi.org/10.1029/2018GL077717

Ladant, J.-B., & Donnadieu, Y. (2016). Palaeogeographic regulation of glacial events during the Cretaceous supergreenhouse. *Nature Communications*, *7*, 1–9. https://doi.org/10.1038/ncomms12771

Lunt, D. J., Dunkley Jones, T., Heinemann, M., Huber, M., LeGrande, A., Winguth, A., et al. (2012). A model-data comparison for a multi-model ensemble of early Eocene atmosphere-ocean simulations: EoMIP. *Climate of the Past*, *8*(5), 1717–1736.

Lunt, D. J., Farnsworth, A., Loptson, C., Foster, G. L., Markwick, P., O'Brien, C. L., et al. (2016). Palaeogeographic controls on climate and proxy interpretation. *Climate of the Past*, *12*(5), 1181–1198.

Lunt, D. J., Haywood, A. M., Schmidt, G. A., Salzmann, U., Valdes, P. J., & Dowsett, H. J. (2010). Earth system sensitivity inferred from Pliocene modelling and data. *Nature Geoscience*, *3*, 60–64.

MacLeod, K., Martin, E. E., & Blair, S. W. (2008). Nd isotopic excursion across Cretaceous ocean anoxic event 2 (Cenomanian-Turonian) in the tropical North Atlantic. *Geology*, *36*, 811–814.

Markwick, P. J. (2007). Deep time perspectives on climate change: Marrying the signal from computer models and biological proxies. In M, M. Williams, A. M. Haywood, J. F. Gregory, & D. N. Schmidt (Eds.), *chap. The palaeogeographic and palaeoclimatic significance of climate proxies for data-model comparisons*. London, UK: The Micropalaeontological Society Special Publications, Geological Society of London.

Martínez-Botí, M., Foster, G., Chalk, T., Rohling, E., Sexton, P., Lunt, D., et al. (2015). Plio-Pleistocene climate sensitivity evaluated using high-resolution CO_2 records. *Nature*, *518*, 49–54.

Moss, R. H., Edmonds, J. A., Hibbard, K. A., Manning, M. R., Rose, S. K., van Vuuren, D. P., et al. (2010). The next generation of scenarios for climate change research and assessment. *Nature*, *463*, 747–756.

Müller, R. D., Sdrolias, M., Gaina, C., Steinberger, B., & Heine, C. (2008). Long-term sea-level fluctuations driven by ocean basin dynamics. *Science*, *319*, 1357–1362. https://doi.org/10.1126/science.1151540

O'Brien, C. L., Robinson, S. A., Pancost, R. D., Damsté, S., Schouten, S., Lunt, D. J., et al. (2017). Cretaceous sea-surface temperature evolution: Constraints from TEX_{86} and planktonic foraminiferal oxygen isotopes. *Earth Science Reviews*, *172*, 224–247.

PALAEOSENS Project Members (2012). Making sense of palaeoclimate sensitivity. *Nature*, *491*, 683–691.

Pohl, A., Donnadieu, Y., Le Hir, G., Buoncristiani, J.-F., & Vennin, E. (2014). Effect of the Ordovician paleogeography on the (in)stability of the climate. *Climate of the past*, *10*(6), 2053–2066. Retrieved from https://doi.org/10.5194/cp-10-2053-2014

Pohl, A., Laugie, M., Borgomano, J., Michel, J., Lanteaume, C., Scotese, C. R., et al. (2019). Quantifying the paleogeographic driver of Cretaceous carbonate platform development using paleoecological niche modeling. *Palaeogeography, Palaeoclimatology, Palaeoecology*, *514*, 222–232. https://doi.org/10.1016/j.palaeo.2018.10.017

Rogelj, J., Meinshausen, M., Sedlacek, J., & Knutti, R. (2014). Implications of potentially lower climate sensitivity on climate projections and policy. *Environmental Research Letters*, *9*, 031003. https://doi.org/10.1088/1748-9326/9/3/031003

Rohling, E. J., Marino, G., Foster, G. L., Goodwin, P. A., von der Heydt, A. S., & Kohler, P. (2018). Comparing climate sensitivity, past and present. *Annual Review of Marine Science*, *10*, 261–288.

Schmidt, G. A., Annan, J. D., Bartlein, P. J., Cook, B. I., Guilyardi, E., Hargreaves, J. C., et al. (2014). Using palaeo-climate comparisons to constrain future projections in CMIP5. *Climate of the Past*, *10*(1), 221–250. Retrieved from https://doi.org/10.5194/cp-10-221-2014

Shaffer, G., Huber, M., Rondanelli, R., & Pepke Pedersen, J. O. (2016). Deep time evidence for climate sensitivity increase with warming. *Geophysical Research Letters*, *43*, 6538–6545. https://doi.org/10.1002/2016GL069243

Sluijs, A., Schouten, S., Pagani, M., Woltering, M., Brinkhuis, H., Damsté, J. S., et al. (2006). Subtropical Arctic Ocean temperatures during the Palaeocene/Eocene thermal maximum. *Nature*, *441*, 610–613.

Sømme, T., Helland-Hansen, W., & Granjeon, D. (2009). Impact of eustatic amplitude variations on shelf morphology, sediment dispersal, and sequence stratigraphic interpretation: Icehouse versus greenhouse systems. *Geology*, *37*(7), 587–590. https://doi.org/10.1130/G25511A.1

Tierney, J. E., Sinninghe Damsté, J. S., Pancost, R. D., Sluijs, A., & Zachos, J. C. (2017). Eocene temperature gradients. *Nature Geoscience*, *10*, 538–539.

Valdes, P. J., Armstrong, E., Badger, M. P. S., Bradshaw, C. D., Bragg, F., Crucifix, M., et al. (2017). The BRIDGE HadCM3 family of climate models: HadCM3@bristol v1.0. *Geoscientific Model Development*, *10*(10), 3715–3743. https://doi.org/10.5194/gmd-10-3715-2017

Zeebe, R. E., Zachos, J. C., & Dickens, G. R. (2009). Carbon dioxide forcing alone insufficient to explain palaeoceneeocene thermal maximum warming. *Nature Geoscience*, *2*, 576–580.